CHEMISTRY OF MATERIALS
Cite This: Chem. Mater. 2019, 31, 826−833
Article
pubs.acs.org/cm

Effective and Noneffective Recombination Center Defects in Cu_2ZnSnS_4: Significant Difference in Carrier Capture Cross Sections

Jiqiang Li,[†,‡] Zhen-Kun Yuan,[†,‡] Shiyou Chen,*[,§] Xin-Gao Gong,*[,†,‡] and Su-Huai Wei[∥]

[†]Department of Physics, Key Laboratory for Computational Physical Science (Ministry of Education), State Key Laboratory of Surface Physics, Fudan University, Shanghai 200433, China

[‡]Collaborative Innovation Center of Advanced Microstructures, Nanjing 210093, Jiangsu, China

[§]Key Laboratory of Polar Materials and Devices (Ministry of Education), East China Normal University, Shanghai 200241, China

[∥]Beijing Computational Science Research Center, Beijing 100193, China

Supporting Information

ABSTRACT: By combining the electron−phonon coupling effect and the static coupling formalism, we calculate, through the first-principles methods, the carrier capture cross sections of the three possible nonradiative recombination center (NRRC) defects in Cu_2ZnSnS_4. These values are currently unavailable but critical for understanding the limiting factors of the minority carrier lifetime and simulating the photovoltaic devices. We show that the cross sections for Sn_{Zn}^{2+} capturing one electron (a (+2/+1) transition) and for $[Cu_{Zn}−Sn_{Zn}]^+$ capturing one electron (a (+1/0) transition) are both very large, whereas for Sn_{Zn}^{+} capturing one electron (a (+1/0) transition) is much smaller by several orders of magnitude. The minority carrier lifetime will be limited to below 1 ns if the concentrations of Sn_{Zn}^{2+} and $[Cu_{Zn}−Sn_{Zn}]^+$ are higher than 10^{15} cm^{-3}, so they are effective NRRCs, whereas the lifetime can be as long as 10 μs with the same concentration of Sn_{Zn}^{+}, so Sn_{Zn}^{+} is a noneffective NRRC. The phonon mode analysis shows that the cross section is strongly correlated with the vibration mode of Sn−S bonds around the defects and its coupling with the localized wavefunction on the defect state. Sn_{Zn}^{2+} and $[Cu_{Zn}−Sn_{Zn}]^+$ have a short and strong Sn−S bond with a high-frequency vibration mode, and these two defects undergo a large structural distortion after capturing an electron, which decreases the barrier for carrier capture and thus produces a large cross section. In contrast, Sn_{Zn}^{+} has a softer Sn−S vibration mode and thus much higher barrier for electron capture. Our calculations not only identify two effective NRRCs, which provide the mechanism behind why the Cu-poor, Zn-rich, Sn-poor growth condition, were widely adopted for fabricating high-efficiency Cu_2ZnSnS_4 solar cells but also show that a very large difference can exist in the carrier capture cross sections for the same defect in different charge states (Sn_{Zn}^{2+} vs Sn_{Zn}^{+}). We propose that the deep-level defects may have large carrier capture cross sections if they are surrounded by strong bonds and undergo considerable structural relaxations after capturing a carrier, which can be used as an empirical criterion for the quick identification of effective NRRCs.

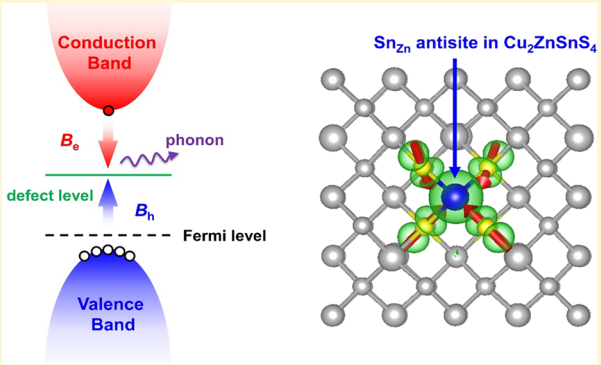

1. INTRODUCTION

The kesterite semiconductors Cu_2ZnSnS_4 and $Cu_2ZnSnSe_4$ have drawn intensive attention as the promising thin-film solar cell materials for their earth-abundant and environment-friendly component elements, ideal band gap (1.5 eV,[1−4] close to the optimal gap for single-junction solar cell),[5] high optical absorption coefficient (>10^4 cm^{-1}),[6] and fabrication techniques compatible to the commercialized $Cu(In,Ga)Se_2$ solar cells.[7] However, its record photovoltaic efficiency (12.6%)[8] was still much lower than the theoretical limit of 32% according to the Shockley−Queisser model,[5] despite the intensive study in the past decade. One critical limit to the efficiency is the short lifetime of minority carriers.[9−16] It is only a few nanoseconds (ns) in Cu_2ZnSnS_4,[7,9,17] significantly shorter than that in the $Cu(In,Ga)Se_2$-based solar cells (>100 ns,[14,18] which can be an important reason for the much higher recorded efficiency 22.6%).[19] Such a short minority carrier lifetime in Cu_2ZnSnS_4 is often attributed to the nonradiative recombination of electron (minority) and hole (majority) carriers induced by the deep-level defects in Cu_2ZnSnS_4, which are the main candidates of the effective recombination centers.[9,11,17,20−23]

Among the varieties of the defects in Cu_2ZnSnS_4, the Sn_{Zn} antisite, and the $Cu_{Zn}−Sn_{Zn}$ cluster are reported to be the possible nonradiative recombination centers (NRRCs). Density functional theory calculations showed that the Sn_{Zn} antisite

Received: September 17, 2018
Revised: January 8, 2019
Published: January 11, 2019

DOI: 10.1021/acs.chemmater.8b03933
Chem. Mater. 2019, 31, 826−833

has deep levels in the band gap.[20,21,23,24] Besides Sn_{Zn}, the Cu_{Zn}–Sn_{Zn} defect cluster also has a deep level as shown by both the calculations[21] and the experiments.[25] Furthermore, the Cu_{Zn}–Sn_{Zn} cluster has a high concentration even in stoichiometric Cu_2ZnSnS_4 samples because its formation energy is largely decreased by the attractive interaction between Cu_{Zn}^{-} and Sn_{Zn}^{2+}. If Sn_{Zn} and Cu_{Zn}–Sn_{Zn} are both effective recombination centers, the minority carrier lifetime and thus the photovoltaic performance of Cu_2ZnSnS_4 solar cell would be limited. Following the Shockley–Read–Hall theory, the deep-level defects with low formation energies are often considered as important candidates of recombination centers.[26,27] However, whether a deep-level defect acts as an effective recombination center depends quantitatively on its carrier capture cross section (CCCS), that is, a deep-level defect is not an effective recombination center if it has a high concentration but a small CCCS. Currently, the CCCSs of Sn_{Zn} and Cu_{Zn}–Sn_{Zn} are still unknown, making it an open question whether the two defects are effective recombination centers. Moreover, the lack of the accurate CCCS values makes it difficult to judge the detrimental influence of such deep-level defects on the minority carrier lifetime and thus the photovoltaic performance quantitatively. Therefore, the accurate determination of CCCSs of defects becomes critical for advancing the defect physics of Cu_2ZnSnS_4 and improving the solar cell performance.

Unfortunately, the experimental measurements and the theoretical calculations of CCCSs of defects are both very challenging in multinary compound semiconductors such as Cu_2ZnSnS_4 or $CH_3NH_3PbI_3$. Experimentally, because there are many possible lattice defects producing a series of defect levels in the band gap of the multinary semiconductors, it is difficult to directly measure the CCCS of a certain defect level.[28–30] Theoretically, the analytic model for the CCCS calculation was developed in 1950s and 1960s.[31–34] However, the direct calculation of CCCS requires the accurate calculation of the defect-induced electron–phonon coupling matrix in practical semiconductors, which was not available for many decades because the ab initio calculation of electron–phonon coupling matrix elements is very time consuming, so the calculated results of CCCSs were usually estimated based on the empirical and approximated electron–phonon coupling matrix and thus debatable with obvious inconsistency with the experiments.[33,35–38] Recently, Shi and Wang[39,40] developed an effective method to calculate the defect-induced electron–phonon coupling matrix and thus the CCCS based on density functional theory calculations, which had been successfully used for calculating the CCCS of deep-level defects in GaN and GaP.[39–41] Further progress has been achieved in the method development and calculations of the CCCS and the nonradiative carrier capture rates of deep-level defects in binary semiconductors[42–46] and even in multinary perovskite $CH_3NH_3PbI_3$.[47] This progress makes it possible for us to calculate the CCCSs of Sn_{Zn} and Cu_{Zn}–Sn_{Zn} in Cu_2ZnSnS_4.

In this work, using the recently developed method,[47] we studied the nonradiative recombination induced by the Sn_{Zn} antisite and the Cu_{Zn}–Sn_{Zn} cluster in Cu_2ZnSnS_4. The CCCSs and the corresponding nonradiative electron capture rates were calculated, which surprisingly shows that both the +2 charged Sn_{Zn}^{2+} and +1 charged $[Cu_{Zn}–Sn_{Zn}]^{+}$ are effective NRRCs, imposing a serious limit to the minority carrier lifetime, whereas the +1 charged Sn_{Zn}^{+} is not an effective NRRC. The microscopic origin of the significant difference results from the different phonons (the vibration mode of Sn–S bonds) around the Sn_{Zn} antisite as well as the different Sn–S bond lengths and strengths (defect phonon frequencies) at different charge states of Sn_{Zn}. The calculated results explain (i) why Cu_2ZnSnS_4 has a short minority carrier lifetime and (ii) why the Cu-poor, Zn-rich, Sn-poor condition is desirable for fabricating high-efficiency Cu_2ZnSnS_4 solar cells. Furthermore, the difference between the effective and noneffective NRRCs inspires us to propose a simple but practical criterion for the quick prediction of effective NRRCs in semiconductors based on the bond lengths near the defects in different charge states.

2. RESULTS AND DISCUSSION

2.1. Calculated CCCSs. The Sn_{Zn} antisite is a donor defect and can be stable in Cu_2ZnSnS_4 at three charge states, 0 (neutral, not ionized), +1, and +2. Its calculated formation energies at different charge states are shown in Figure 1b (the calculation details and the influence of the spin-polarized calculations are discussed in Supporting Information). It produces three transition energy levels that are deep in band gap, that is, the (0/+), (+/2+), and (0/2+) levels, which may act as recombination center levels according to the Shockley–Read–Hall theory.[26,27]

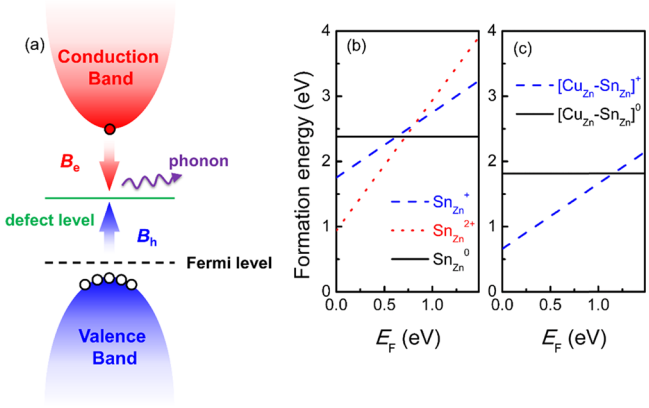

Figure 1. (a) Schematic plot of the nonradiative carrier recombination process. The calculated formation energies of (b) the Sn_{Zn} antisite and (c) the Cu_{Zn}–Sn_{Zn} cluster at different charge states. E_F is the Fermi energy referenced to the VBM level.

In a nonradiative recombination process, a defect state captures one electron carrier from the conduction band minimum (CBM) state and captures one hole carrier from the valence band maximum (VBM) state, leading to the recombination of the electron and hole carriers and the excitation of the phonons, as shown in Figure 1a. Because the synthesized Cu_2ZnSnS_4 samples are always p-type and the Fermi level is near the VBM level, so the donor defect Sn_{Zn} is ionized, usually in the 2+ charge state with energy levels unoccupied by electrons. These unoccupied donor levels can capture electrons from the CBM level. Meanwhile, there are high population of hole carriers in the p-type samples, so the hole carriers can be easily captured by Sn_{Zn} if its donor level is occupied by an electron. Hence, the cross section for Sn_{Zn} capturing an electron carrier (minority carrier in p-type Cu_2ZnSnS_4) is the bottleneck of the whole recombination process. We will focus on the electron capture process in the following discussion.

DOI: 10.1021/acs.chemmater.8b03933
Chem. Mater. 2019, 31, 826–833

Because the possibility for a defect capturing two or more electron carriers simultaneously is small and negligible because of the Coulomb repulsion between two electron carriers, here, only the process of capturing a single electron carrier is taken into account. As mentioned above, only the (+/2+) and (0/+) levels (involve capturing a single electron carrier) are possible electron capture channels of the Sn_{Zn} antisite. Specifically, the +2 charged Sn_{Zn}^{2+} can capture one electron carrier from the CBM and transit into the +1 charged state, inducing a (2+/+) transition, whereas the +1 charged Sn_{Zn}^{+} can capture one electron carrier from the CBM and transit into the neutral state, inducing a (+/0) transition.

Similarly, the calculated formation energies of the Cu_{Zn}−Sn_{Zn} cluster at different charge states are shown in Figure 1c. Our calculated Cu_{Zn}−Sn_{Zn} (0/+) level is 1.16 eV above the VBM. The +1 charged $[Cu_{Zn}-Sn_{Zn}]^{+}$ can capture one electron carrier from the CBM and transit into the neutral state, inducing a (+/0) transition. Compared with Sn_{Zn}^{2+}, $[Cu_{Zn}-Sn_{Zn}]^{+}$ has a lower formation energy because of the attractive interaction between Cu_{Zn}^{-} and Sn_{Zn}^{2+}; hence, $[Cu_{Zn}-Sn_{Zn}]^{+}$ has a concentration nearly four orders of magnitude higher than Sn_{Zn}^{2+} at 300 K if the Fermi level is located at the VBM.

At 300 K, the electron capture rate of Sn_{Zn}^{2+} in Cu_2ZnSnS_4 is calculated as $B_e(Sn_{Zn}^{2+}) = 2.4 \times 10^{-6}$ cm^3/s (the (+2/+1) transition). The corresponding electron capture cross section is $\sigma_e(Sn_{Zn}^{2+}) = 8.8 \times 10^{-14}$ cm^2, which is relatively large compared with those of the common defects (or impurities) in the conventional semiconductors, for example, the In impurity in Si (4×10^{-17} cm^2)[36] and the Zn impurity in Si (1×10^{-19} cm^2).[37] Actually, our calculated $\sigma_e(Sn_{Zn}^{2+})$ is close to the upper limit of the experimental cross sections for the defects in a wide variety of semiconductors (10^{-21}−10^{-13} cm^2).[37,48]

In contrast, the electron capture rate of Sn_{Zn}^{+} is nearly four orders of magnitude smaller, that is, $B_e(Sn_{Zn}^{+}) = 1.3 \times 10^{-10}$ cm^3/s (the (+1/0) transition), and the corresponding cross section is $\sigma_e(Sn_{Zn}^{+}) = 4.7 \times 10^{-18}$ cm^2. There are two major factors accounting for its smaller electron capture rate: (i) the energy barrier of the (+/0) transition is much higher than that of the (2+/+) transition, as discussed in Section 2.3 and (ii) the attractive interaction of the +1 charged center on electron carriers is weaker than that of the +2 charged center. Considering the much smaller electron capture rate of the (+/0) transition and the lower concentration (due to the higher formation energy in p-type Cu_2ZnSnS_4) of Sn_{Zn}^{+}, the electron capture process through (+2/+) transition of Sn_{Zn}^{2+} is the main electron capture channel of the Sn_{Zn} antisite.

At 300K, $[Cu_{Zn}-Sn_{Zn}]^{+}$ has an electron capture rate close to Sn_{Zn}^{2+}, $B_e([Cu_{Zn} - Sn_{Zn}]^{+}) = 1.2 \times 10^{-6}$ cm^3/s (+/0 transition) and $\sigma_e([Cu_{Zn} - Sn_{Zn}]^{+}) = 4.5 \times 10^{-14}$ cm^2. The values are on the same order of magnitude as that of Sn_{Zn}^{2+}. This similarity is mainly attributed to their similar energy barriers, as discussed in Section 2.3. $\sigma_e([Cu_{Zn} - Sn_{Zn}]^{+})$ is also close to the upper limit of the measured cross sections for the defects in various semiconductors.[37,48] Considering its lower formation energy (thus a higher concentration) than Sn_{Zn}^{2+}, $[Cu_{Zn}-Sn_{Zn}]^{+}$ may be a more effective recombination center defect and its detrimental influence on the photovoltaic performance is expected to be even more significant.

2.2. Limit to the Minority Carrier Lifetime. With the calculated electron capture rates, we can now calculate the limit to the minority carrier lifetime imposed by Sn_{Zn}^{2+} and $[Cu_{Zn}-Sn_{Zn}]^{+}$ in Cu_2SnZnS_4. The dependence of the maximum lifetime of an electron carrier (minority carrier) on the concentrations of Sn_{Zn}^{2+} and $[Cu_{Zn}-Sn_{Zn}]^{+}$ is shown in Figure 2. The maximum lifetime of an electron carrier τ_e typically decreases with the defect concentration N_D as $\tau_e = \frac{1}{B_e N_D}$.

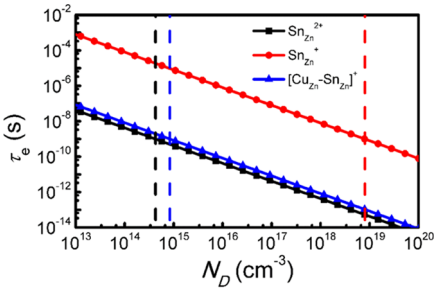

Figure 2. Dependence of the maximum lifetimes of minority carriers (electrons) on the concentrations of Sn_{Zn}^{2+}, Sn_{Zn}^{+}, and $[Cu_{Zn}-Sn_{Zn}]^{+}$ in Cu_2ZnSnS_4. The dashed lines show the concentration of the three defects above which the minority carrier lifetime will be lower than 1 ns.

According to our calculations, the minority carrier lifetime in Cu_2ZnSnS_4 would be limited to lower than 0.4 ns, 8 μs, or 0.8 ns, respectively, if the concentration of Sn_{Zn}^{2+}, Sn_{Zn}^{+}, or $[Cu_{Zn}-Sn_{Zn}]^{+}$ is higher than 10^{15} cm^{-3}. On the other hand, to obtain a minority carrier lifetime longer than ~1 ns (close to the experimentally measured lifetime)[7,9,17] in Cu_2ZnSnS_4, the concentrations of Sn_{Zn}^{2+}, Sn_{Zn}^{+} antisite, or $[Cu_{Zn}-Sn_{Zn}]^{+}$ cluster should be lower than $N_D = \frac{1}{B_e\tau_e} = 4.2 \times 10^{14}$, 8.0×10^{18}, or 8.3×10^{14} cm^{-3}, respectively, as denoted by the dashed lines in Figure 2.

In our previous works, we showed that concentration of $[Cu_{Zn}-Sn_{Zn}]^{+}$ at 300 K could be as high as 10^{15} cm^{-3} even in stoichiometric samples.[21] According to the discussion above, the Cu_{Zn}−Sn_{Zn} cluster is definitely an effective recombination center even in stoichiometric samples and its detrimental influence becomes more serious in the nonstoichiometric sample grown under the Cu-rich, Zn-poor, Sn-rich condition because of the higher concentration. Although the Sn_{Zn}^{2+} antisite has a higher formation energy and a lower concentration, such a large electron capture rate (exceeding 10^{-6} cm^3/s) makes the Sn_{Zn} antisite another effective recombination center and its detrimental effect can be serious especially in the nonstoichiometric sample grown under the Cu-rich, Zn-poor, Sn-rich condition. As a result, both $[Cu_{Zn}-Sn_{Zn}]^{+}$ and Sn_{Zn}^{2+} act as effective recombination centers in Cu_2ZnSnS_4 samples grown under the Cu-rich, Zn-poor, Sn-rich condition and can significantly reduce the minority carrier lifetime (thus the photovoltaic performance). Therefore, the Cu-poor, Zn-rich, Sn-poor condition is preferable for a high-efficiency Cu_2SnZnS_4 solar cell, which is consistent with the experimental observation that all the kesterite solar cells with reported efficiencies higher than 8% have the elemental ratios of Cu/(Zn + Sn) ≈ 0.8 and Zn/Sn ≈ 1.2.[7,49−52]

2.3. Microscopic Origin of Large Electron Capture Rates. Because Sn_{Zn}^{2+} and $[Cu_{Zn}-Sn_{Zn}]^{+}$ are effective recombination center defects, it is of fundamental interest to reveal the microscopic origin of large electron capture rates (cross sections), which may help us identify other defects that may act as effective recombination centers. The electron capture rate is calculated as $B_e = f_S\tilde{B}_e$,[43] where f_S is a system-

DOI: 10.1021/acs.chemmater.8b03933
Chem. Mater. 2019, 31, 826−833

dependent factor,[53] representing attractive interaction between the positively charged defect and the electron carriers, and $\tilde{B}_e$ is the transition rate between different electronic states. In general, the variance of f_S for different systems at the same temperature is small (not by several orders of magnitude). Therefore, the differences in electron capture rates are mainly attributed to the variation of the transition rates $\tilde{B}_e$.

Because the nonradiative transition across different electronic states is accompanied by the multiphonon emission,[39,48] a clear understanding of the lattice dynamics, electronic structure, and the electron−phonon coupling in Cu_2ZnSnS_4 system is necessary for understanding the variation of $\tilde{B}_e$. The calculated phonon density of states (DOS) of the supercell with Sn_{Zn}^{2+} is shown in Figure 3. The phonon energies

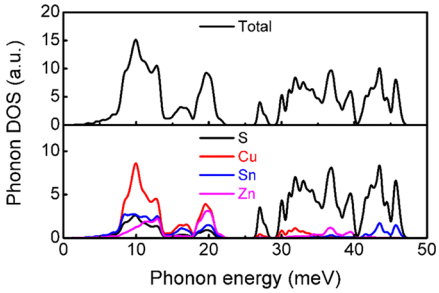

Figure 3. Total (up panel) and projected (down panel) phonon DOS of the 64-atom Cu_2ZnSnS_4 supercell with a Sn_{Zn}^{2+} antisite.

(frequencies) range from 0 to 50 meV. The projected phonon DOS on different component elements shows that the high-frequency phonon modes are mainly contributed by the light element *S*, whereas all other elements contribute to the low-frequency phonon modes. The phonon DOS of the supercell with a Sn_{Zn}^{+} antisite or a $[Cu_{Zn}-Sn_{Zn}]^{+}$ cluster is similar.

In Figure 4c,f,i, we plotted the transition rates $\tilde{B}_e$ projected on different phonon modes (as a function of the phonon energy) of the supercells with a Sn_{Zn}^{2+} antisite, a Sn_{Zn}^{+} antisite, and a $[Cu_{Zn}-Sn_{Zn}]^{+}$ cluster. Interestingly, the transition rates $\tilde{B}_e$ are contributed mainly by the phonon modes in a very

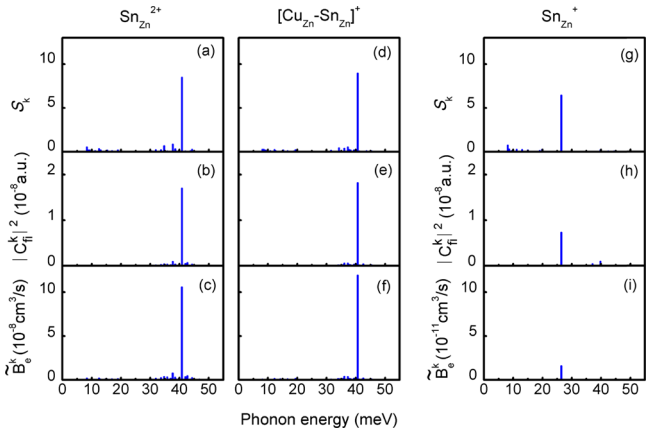

Figure 4. The contribution of different phonon modes to the (a,d,g) Huang−Rhys factors S_k, (b,e,h) squared norms of the electron−phonon coupling matrix elements $|C_{fi}^k|^2$, and (c,f,i) electronic state transition rates $\tilde{B}_e^k$ at 300 K. The left column is for the supercell with a Sn_{Zn}^{2+} antisite, the middle column is for the supercell with a $[Cu_{Zn}-Sn_{Zn}]^{+}$ cluster, and the right column is for the supercell with a Sn_{Zn}^{+} antisite.

narrow frequency range (41 meV for Sn_{Zn}^{2+} and $[Cu_{Zn}-Sn_{Zn}]^{+}$ and 26 meV for Sn_{Zn}^{+}), whereas the contribution of other phonon modes is negligible. It can be understood according to the Huang−Rhys factor $S_k = \frac{\omega_k}{2\hbar}\Delta Q_k^{\ 2}$ (Figure 4a,d,g) and the electron−phonon coupling matrix elements $\langle\psi_f|\frac{\partial H}{\partial Q_k}|\psi_i\rangle$ (abbreviated as $|C_{fi}^k|^2$) (Figure 4b,e,h), which can also be projected on the phonon modes as a function of the frequency. Huang−Rhys factors show that these modes in the narrow frequency range dominate the lattice relaxation accompanying the electronic transition (carrier capture), which implies that the energy change in the electronic transition is converted into the lattice thermal energy mainly by exciting these phonon modes. On the other hand, the electron−phonon coupling matrix elements shown in Figure 4b,e,h suggest that these phonon modes couple the initial and final states of the electronic transition efficiently, which increases the electronic transition rates.

To reveal the origin of these phonon modes (with an energy of 41 meV for Sn_{Zn}^{2+} and $[Cu_{Zn}-Sn_{Zn}]^{+}$ and 26 meV for Sn_{Zn}^{+}), we plot the squared norms of their eigenvectors $|e_k(R)|^2$ projected on the different atoms (with the red arrows showing the vibration of different atoms) in Figure 5. The vibration

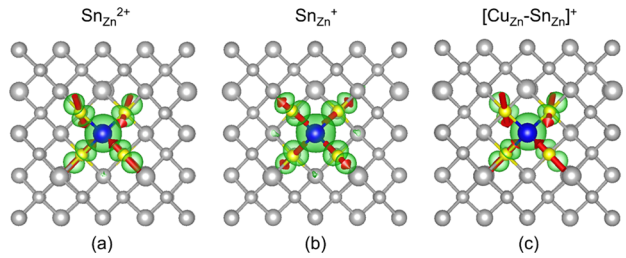

Figure 5. The phonon modes and the electronic states induced by the defects (a) Sn_{Zn}^{2+}, (b) Sn_{Zn}^{+}, and (c) $[Cu_{Zn}-Sn_{Zn}]^{+}$. The green isosurfaces represent the squared norms of wavefunctions of the transition energy levels of defects, whereas the red arrows denote the vibration of the S atoms (marked in yellow) around the Sn_{Zn} antisite (marked in blue) associated with the defect phonon mode (with an energy of 41 meV for Sn_{Zn}^{2+} and $[Cu_{Zn}-Sn_{Zn}]^{+}$ and 26 meV for Sn_{Zn}^{+}).

amplitude, $|e_k(R)|^2$, of the four S atoms around the Sn_{Zn} ansite is much larger than those of other atoms, indicating that these phonon modes are mainly localized on the four S atoms. The vibration direction of the four S atoms shows that these phonon modes are actually the vibration of the Sn−S bonds around the Sn_{Zn} antisite. Therefore, the lattice relaxation (ΔQ_k) caused by the carrier capture process is mainly accommodated by the elongation of the four Sn−S bonds around the Sn_{Zn} antisite.

Because the electronic states of the Sn_{Zn} (+2/+) and (+/0) and $Cu_{Zn}-Sn_{Zn}$ (+/0) transition energy levels are also localized around these defects (as shown by the wavefunction isosurface in Figure 5), the overlapping of the electronic and phonon states makes their coupling strong. In this way, we can understand why the electron−phonon coupling matrix elements $\langle\psi_f|\frac{\partial H}{\partial Q_k}|\psi_i\rangle$ are large for these defect-induced phonon modes.

Now, we have identified the origin of the phonon modes that determine the CCCSs of Sn_{Zn}^{2+}, Sn_{Zn}^{+}, and $[Cu_{Zn}-Sn_{Zn}]^{+}$, but one open question is why the cross section of Sn_{Zn}^{+} is

DOI: 10.1021/acs.chemmater.8b03933
Chem. Mater. 2019, 31, 826−833

much smaller than those of Sn_{Zn}^{2+} and $[Cu_{Zn}-Sn_{Zn}]^{+}$. Does this significant difference result from their different phonon modes?

Compared with the phonon modes of Sn_{Zn}^{2+} and $[Cu_{Zn}-Sn_{Zn}]^{+}$ (with an energy of 41 meV), the phonon mode of Sn_{Zn}^{+} has a much lower energy (26 meV). Because the phonon mode is mainly the vibration of the Sn−S bonds, the large difference in the phonon energy can be attributed to the Sn−S bond difference, as listed in Table 1. The length of Sn−S bond

Table 1. Sn−S Bond Lengths, Defect Phonon Energy $\hbar\omega_{def}$, Electronic Transition Energy ΔE (Relative to the CBM Level), and Electronic Transition Energy Barriers E_b for the Defects Sn_{Zn}^{2+}, Sn_{Zn}^{+}, and $[Cu_{Zn}-Sn_{Zn}]$[a]

defects	bond length (Å)	$\hbar\omega_{def}$ (meV)	ΔE (eV)	E_{rel} (eV)	E_b (eV)
Sn_{Zn}^{2+}	2.43	41	0.67	0.50	0.01
Sn_{Zn}^{+}	2.57	26	0.86	0.23	0.44
Sn_{Zn}^{0}	2.71				
$[Cu_{Zn}-Sn_{Zn}]^{+}$	2.43/2.44	41	0.33	0.52	0.02
$[Cu_{Zn}-Sn_{Zn}]^{0}$	2.57/2.58				

[a]The Sn−S bond lengths of neutral Sn_{Zn}^{0} and $[Cu_{Zn}-Sn_{Zn}]^{0}$ are also listed for comparison.

around the Sn_{Zn} antisite changes as the charge state of the defect changes, that is, it increases from 2.43 Å around +2 charged Sn_{Zn}^{2+} to 2.57 Å around +1 charged Sn_{Zn}^{+} and then to 2.71 Å around neutral Sn_{Zn}^{0}. The bond length increase is consistent with the change of the valence state of Sn. Sn takes the nominal +4 ionized state for Sn_{Zn}^{2+}, so the Coulomb attraction between Sn and S in the nominal −2 ionized state is large. When Sn captures one (two) electron(s) and changes into Sn_{Zn}^{+} (Sn_{Zn}^{0}), the Coulomb attraction becomes less, so the Sn−S bond becomes longer. The elongation of the Sn−S bond weakens the Sn−S bonds and thus soften the Sn−S vibration mode, resulting the decrease of the defect phonon energy $\hbar\omega_{def}$ from 41 meV of Sn_{Zn}^{2+} to 26 meV of Sn_{Zn}^{+}.

For the defect cluster $Cu_{Zn}-Sn_{Zn}$, Sn takes the +4 ionized state for the +1 charged $[Cu_{Zn}-Sn_{Zn}]^{+}$ and takes the +3 ionized state for the neutral $[Cu_{Zn}-Sn_{Zn}]^{0}$. Therefore, the Sn−S bond length around $[Cu_{Zn}-Sn_{Zn}]^{+}$ is very close to that around Sn_{Zn}^{2+}, and the Sn−S bond length around $[Cu_{Zn}-Sn_{Zn}]^{0}$ is very close to that around Sn_{Zn}^{+}. The similar bond lengths result in the similar phonon energy between $[Cu_{Zn}-Sn_{Zn}]^{+}$ and Sn_{Zn}^{2+}. Our following discussion will show that the similar phonon energies determined the similar electron capture rates of $[Cu_{Zn}-Sn_{Zn}]^{+}$ and Sn_{Zn}^{2+}.

To reveal how the Sn−S bond lengths and the defect phonons determine the electronic transition rate (electron capture rate), we plot the configuration coordinate diagram for both Sn_{Zn}^{2+} (the (2+/+) transition) and Sn_{Zn}^{+} (the (+/0) transition), as shown in Figure 6. The electronic transition energy ΔE is equal to the energy difference between the CBM level and the transition energy levels of defects, that is, ΔE = 0.67 eV for the electron capture of Sn_{Zn}^{2+} because the (2+/+) level is 0.67 eV below the CBM and ΔE = 0.86 eV for the electron capture of Sn_{Zn}^{+} because the (+/0) level is 0.86 eV below the CBM. E_b is the energy barrier for the electronic state transition. The electronic state transition rate $\tilde{B}_e$ depends on E_b, following approximately $\tilde{B}_e = \tilde{B}_0 + \tilde{B}_1 \exp(-E_b/k_BT)$.[42] Following the harmonic model, we can calculate E_b from the lattice relaxation energy, following $E_b = \frac{(\Delta E - E_{rel})^2}{4E_{rel}}$,

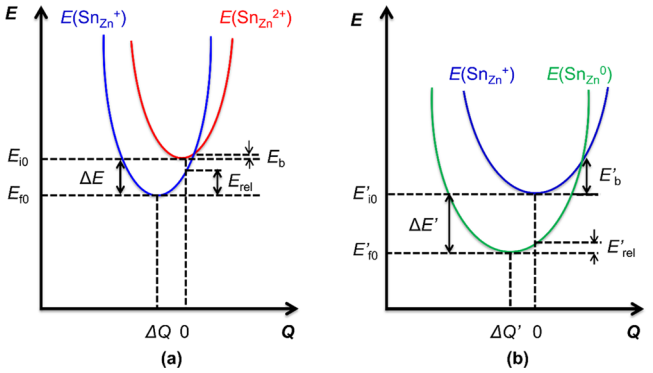

Figure 6. Configuration coordinate diagram (under the harmonic approximation) of the nonradiative electronic state transition for (a) +2 charged Sn_{Zn}^{2+} captures an electron and transforms to +1 charged Sn_{Zn}^{+} and (b) +1 charged Sn_{Zn}^{+} captures an electron and transforms to neutral Sn_{Zn}^{0}. The nonradiative electronic state transition mainly occurs at the cross point of energy curves,[33] it is necessary for a system to overcome energy barrier E_b with the help of phonons. $\Delta E = E_{i0} - E_{f0}$ is the electronic energy difference at the equilibrium states, and ΔQ corresponds to the difference in the equilibrium coordinates between the initial and final states. Lattice relaxation energy, E_{rel}, originates from the equilibrium configuration coordinate difference between the initial and final states.

where $E_{rel} = \sum_k \frac{1}{2}\omega_k^2 \Delta Q_k^2 = \sum_k S_k \hbar\omega_k$ is the lattice relaxation energy in the electronic state transitions, ω_k is the frequency of the phonon modes, and Δ is the coordination difference between the initial and final states.[33,47,54] Because we can calculate both the defect-induce phonon frequencies and the coordination change as the electronic transition occurs, we can calculate E_{rel} and thus E_b, as shown in Table 1.

The calculated energy barriers E_b for Sn_{Zn}^{2+}, Sn_{Zn}^{+}, and $[Cu_{Zn}-Sn_{Zn}]^{+}$ capturing an electron are 0.01, 0.44, and 0.02 eV, respectively. As we can see, the barrier for Sn_{Zn}^{+} capturing an electron is much higher than those for Sn_{Zn}^{2+} and $[Cu_{Zn}-Sn_{Zn}]^{+}$, so we can attribute the much lower transition rate of the Sn_{Zn}^{+} (+/0) transition to its higher energy barrier around 0.44 eV. In contrast, the barriers are only 0.01−0.02 eV for Sn_{Zn}^{2+} and $[Cu_{Zn}-Sn_{Zn}]^{+}$ capturing an electron, explaining their higher transition rates. Based on the energy barrier difference, we explained why Sn_{Zn}^{+} has a much lower electron capture rate than Sn_{Zn}^{2+} and $[Cu_{Zn}-Sn_{Zn}]^{+}$, and now the problem is changed into why their energy barriers differ so significantly.

As mentioned above, the energy barrier of the electronic transition depends on the lattice relaxation energy, E_{rel}, following $E_b = \frac{(\Delta E - E_{rel})^2}{4E_{rel}}$.[47] Usually $\Delta E > E_{rel}$ and E_{rel} is positive, so E_b decreases as E_{rel} increases. Our calculated E_{rel} of Sn_{Zn}^{2+} (0.50 eV) is much larger than that of Sn_{Zn}^{+} (0.23 eV), as shown in Table 1, so we can attribute their energy barrier difference to the relaxation energy difference.

The lattice relaxation energy E_{rel} depends directly on the lattice relaxation and the defect phonon energies, following $E_{rel} = \sum_k \frac{1}{2}\omega_k^2 \Delta Q_k^2 = \sum_k S_k \hbar\omega_k$.[33,54] Our calculated Huang−Rhys factors $S_k = \frac{\omega_k}{2\hbar}\Delta Q_k^2$ in Figure 4a,d,g show that the defect phonon modes at 41 meV (for Sn_{Zn}^{2+}) and 26 meV (for Sn_{Zn}^{+}) dominate the lattice relaxation when Sn_{Zn}^{2+} or Sn_{Zn}^{+} captures an electron, whereas the contribution of other phonon modes is negligible, so the lattice relaxation is in fact

DOI: 10.1021/acs.chemmater.8b03933
Chem. Mater. 2019, 31, 826−833

just the elongation of the Sn−S bonds around the Sn_{Zn} antisite. The coordination change can thus be simplified to the Sn−S bond length change. Because the Sn−S bond lengths increase significantly from 2.43 to 2.57 Å when Sn_{Zn}^{2+} captures an electron, the corresponding coordination change ΔQ for the (2+/+) transition of Sn_{Zn}^{2+} is large. Meanwhile, the Sn−S bonds around Sn_{Zn}^{2+} are short and strong, so the vibration mode of Sn−S bonds have a high energy ($\hbar\omega_{def}$ = 41 meV). The combination of the large coordination change ΔQ and the high defect phonon energy $\hbar\omega_{def}$ leads to a large lattice relaxation energy E_{rel} and thus a low energy barrier E_b for the (2+/+) transition of Sn_{Zn}^{2+}. In contrast, although the (+/0) transition of Sn_{Zn}^{+} has a large Sn−S bond length increase and thus a large ΔQ too, the Sn−S bonds around Sn_{Zn}^{+} are longer and softer, so the defect phonon energy is lower ($\hbar\omega_{def}$ = 26 meV), which decreases its E_{rel} and increases E_b. Now, we understand why Sn_{Zn}^{+} has a much higher energy barrier and lower cross section for capturing an electron carrier than Sn_{Zn}^{2+} and correlated this difference to the bond length difference of Sn−S bonds around them.

Compared to Sn_{Zn}^{2+}, $[Cu_{Zn}-Sn_{Zn}]^{+}$ has a similar Sn−S bond length (~2.43 Å), a similar defect phonon energy and a similar Sn−S bond length increase when it captures an electron, so the lattice relaxation energy and the energy barrier for the (+/0) transition of $[Cu_{Zn}-Sn_{Zn}]^{+}$ are also similar to that of Sn_{Zn}^{2+}. Then, we understand why their electron capture rates are both very high and close to each other ($B_e(Sn_{Zn}^{2+}) = 2.4 \times 10^{-6}$ cm^3/s, and $B_e([Cu_{Zn} - Sn_{Zn}]^{+}) = 1.2 \times 10^{-6}$ cm^3/s).

Our above analysis showed that the bond length change around the defect is a characteristic quality correlating with the coordinate change ΔQ (lattice relaxation) in the carrier capture process, and the bond strength is another characteristic quality correlating with the defect phonon energies, $\hbar\omega_{def}$, so they have important influence on the CCCSs of defects. When the bonds around the defect are short, they are usually strong and their vibration modes have high energies. Therefore, if a defect has short bonds around it and exhibits a large bond length change when it captures a carrier, we can predict empirically that the defect may have a high CCCS and act as an effective recombination center. This may provide a simple but practical criterion for the quick identification of the effective recombination center defects in semiconductors. For multinary compound semiconductors, there may be a large amount of deep-level defects, this simple but practical criterion can save a lot of computational time compared with the complicated and expensive ab initio calculations of nonradiative CCCSs.

3. CONCLUSIONS

We calculated the nonradiative electron capture cross sections of the Sn_{Zn} antisite and the $Cu_{Zn}-Sn_{Zn}$ cluster in kesterite Cu_2ZnSnS_4 through combining the static coupling formalism with a new first-principles method for the electron-phonon coupling matrix. The calculations showed that electron capture cross sections of the +2 charged Sn_{Zn}^{2+} antisite and the +1 charged $[Cu_{Zn}-Sn_{Zn}]^{+}$ cluster are both very large, and they can limit the minority carrier lifetime below 1 ns if their concentrations is higher than 10^{15} cm^{-3}, so they are effective NRRCs. In contrast, the cross section of +1 charged Sn_{Zn}^{+} is much smaller, so it is not an effective NRRC. The large cross sections of Sn_{Zn}^{2+} and $[Cu_{Zn}-Sn_{Zn}]^{+}$ are mainly contributed by the high-frequency vibration phonon of the short and strong Sn−S bonds near the Sn_{Zn} antisite and the large lattice relaxation (Sn−S bond elongation) when they capture an electron. Because the Sn−S bonds become longer and softer near Sn_{Zn}^{+}, its electron capture cross section becomes much smaller. The quantitative identification of the two effective NRRCs explains why the minority carrier lifetime of Cu_2ZnSnS_4 is much shorter than that of $Cu(In,Ga)Se_2$ and also explains why the Cu-poor, Zn-rich, Sn-poor growth condition were widely adopted for fabricating high-efficiency Cu_2ZnSnS_4 solar cells. The analysis on the differences between the effective and noneffective NRRCs (Sn_{Zn}^{2+} vs Sn_{Zn}^{+}) inspires us to propose a simple but practical criterion for the quick identification of effective NRRCs in semiconductors, that is, the deep-level defects surrounded by strong chemical bonds and with considerable lattice relaxations between different charged states may have large nonradiative CCCSs and are potential NRRCs.

Calculation Methods. The static coupling formalism[40,47] is used to describe the non-radiative carrier capture process and to calculate the electronic state transition rate $\tilde{B}_e$. The attractive interaction on electron carriers by the positively charged center is considered through the Sommerfeld factor f_S,[53] giving rise to the carrier capture rate $B_e = f_S\tilde{B}_e$[43] and the corresponding cross section σ_e.

The 64-atom supercells of kesterite Cu_2ZnSnS_4 and the Heyd−Scuseria−Ernzerhof hybrid functional[55,56] are used in all the calculations. Twenty-five percent of the Perdew−Burke−Ernzerhof exchange functional[57] is replaced by the screened Hartree−Fock exchange and the screening parameter is set to 0.2 Å^{-1}. The calculations of structural relaxation and phonon spectrum are performed with the Vienna ab initio simulation package[58] with the projected augmented-wave pseudopotentials,[59] and the cutoff of the plane-wave basis is 400 eV. The lattice structures are relaxed until the atomic forces are smaller than 0.01 eV/Å. The electron−phonon coupling matrix elements are calculated by Quantum Espresso[60] with the finite difference method, where the norm-conserving pseudopotentials are employed and an energy cutoff of 90 Ry is set for the plane-wave basis. The defect transition energy levels are calculated following a standard procedure,[61,62] in which the potential alignment and the finite size-cell effect[63] are considered to correct the formation energies of defects. Because the strong exchange effect in the spin-polarized hybrid functional calculations causes a very large splitting of the occupied spin-up level and the unoccupied spin-down level, thus predicting incorrect transition energy levels and unphysical magnetic moment around the defect with partially occupied defect levels, we performed only the nonspin-polarized hybrid functional calculations. More calculation details including the differences between the spin-polarized and nonspin-polarized hybrid functional calculations are presented in Supporting Information.

■ ASSOCIATED CONTENT

Supporting Information

The Supporting Information is available free of charge on the ACS Publications website at DOI: 10.1021/acs.chemmater.8b03933.

Theoretical formalism for nonradiative CCCS and calculation details of defect transition energy levels and electron−phonon coupling matrix elements (PDF)

DOI: 10.1021/acs.chemmater.8b03933
Chem. Mater. 2019, 31, 826−833

AUTHOR INFORMATION

Corresponding Authors

*E-mail: chensy@ee.ecnu.edu.cn (S.C.).
*E-mail: xggong@fudan.edu.cn (X.-G.G.).

ORCID

Shiyou Chen: 0000-0002-4039-8549
Su-Huai Wei: 0000-0003-1563-4738

Notes

The authors declare no competing financial interest.

ACKNOWLEDGMENTS

This work was supported by the National Key Research and Development Program of China (2016YFB0700700), the Science Challenge Project (TZ2018004), the National Nature Science Foundation of China (NSFC), and the Supercomputer Center of Fudan University. S.C. is supported by NSFC under grant nos. 61574059 and 61722402, the Shu-Guang program (15SG20), the Fok Ying Tung Education Foundation, and the Computer Center of ECNU. S.-H.W is supported by NSFC under grant nos. 51672023, 11634003, and U1530401 and the Science Challenge Project under grant no. TZ20160003.

REFERENCES

(1) Kamoun, N.; Bouzouita, H.; Rezig, B. Fabrication and characterization of Cu_2ZnSnS_4 thin films deposited by spray pyrolysis technique. *Thin Solid Films* **2007**, *515*, 5949−5952.

(2) Tanaka, T.; Nagatomo, T.; Kawasaki, D.; Nishio, M.; Guo, Q.; Wakahara, A.; Yoshida, A.; Ogawa, H. Preparation of Cu_2ZnSnS_4 thin films by hybrid sputtering. *J. Phys. Chem. Solids* **2005**, *66*, 1978−1981.

(3) Seol, J.-S.; Lee, S.-Y.; Lee, J.-C.; Nam, H.-D.; Kim, K.-H. Electrical and optical properties of Cu_2ZnSnS_4 thin films prepared by rf magnetron sputtering process. *Sol. Energy Mater. Sol. Cells* **2003**, *75*, 155−162.

(4) Katagiri, H.; Saitoh, K.; Washio, T.; Shinohara, H.; Kurumadani, T.; Miyajima, S. Development of thin film solar cell based on Cu_2ZnSnS_4 thin films. *Sol. Energy Mater. Sol. Cells* **2001**, *65*, 141−148.

(5) Shockley, W.; Queisser, H. J. Detailed balance limit of efficiency of *p-n* junction solar cells. *J. Appl. Phys.* **1961**, *32*, 510−519.

(6) Ito, K.; Nakazawa, T. Electrical and optical properties of stannite-type quaternary semiconductor thin films. *Jpn. J. Appl. Phys.* **1988**, *27*, 2094−2097.

(7) Repins, I.; Beall, C.; Vora, N.; DeHart, C.; Kuciauskas, D.; Dippo, P.; To, B.; Mann, J.; Hsu, W.-C.; Goodrich, A.; Noufi, R. Co-evaporated $Cu_2ZnSnSe_4$ films and devices. *Sol. Energy Mater. Sol. Cells* **2012**, *101*, 154−159.

(8) Wang, W.; Winkler, M. T.; Gunawan, O.; Gokmen, T.; Todorov, T. K.; Zhu, Y.; Mitzi, D. B. Device characteristics of CZTSSe thin-film solar cells with 12.6% efficiency. *Adv. Energy Mater.* **2014**, *4*, 1301465.

(9) Kumar, M.; Dubey, A.; Adhikari, N.; Venkatesan, S.; Qiao, Q. Strategic review of secondary phases, defects and defect-complexes in kesterite CZTS−Se solar cells. *Energy Environ. Sci.* **2015**, *8*, 3134−3159.

(10) Polizzotti, A.; Repins, I. L.; Noufi, R.; Wei, S.-H.; Mitzi, D. B. The state and future prospects of kesterite photovoltaics. *Energy Environ. Sci.* **2013**, *6*, 3171−3182.

(11) Polman, A.; Knight, M.; Garnett, E. C.; Ehrler, B.; Sinke, W. C. Photovoltaic materials: Present efficiencies and future challenges. *Science* **2016**, *352*, aad4424.

(12) Ghorpade, U.; Suryawanshi, M.; Shin, S. W.; Gurav, K.; Patil, P.; Pawar, S.; Hong, C. W.; Kim, J. H.; Kolekar, S. Towards environmentally benign approaches for the synthesis of CZTSSe nanocrystals by a hot injection method: a status review. *Chem. Commun.* **2014**, *50*, 11258−11273.

(13) Repins, I. L.; Romero, M. J.; Li, J. V.; Wei, S.-H.; Kuciauskas, D.; Jiang, C.-S.; Beall, C.; DeHart, C.; Mann, J.; Hsu, W.-C.; Teeter, G.; Goodrich, A.; Noufi, R. Kesterite successes, ongoing work, and challenges: a perspective from vacuum deposition. *IEEE J. Photovoltaics* **2013**, *3*, 439−445.

(14) Repins, I. L.; Metzger, W. K.; Perkins, C. L.; Li, J. V.; Contreras, M. A. Correlation Between Measured Minority-Carrier Lifetime and $Cu(In,Ga)Se_2$ Device Performance. *IEEE Trans. Electron Devices* **2010**, *57*, 2957−2963.

(15) Metzger, W. K.; Albin, D.; Levi, D.; Sheldon, P.; Li, X.; Keyes, B. M.; Ahrenkiel, R. K. Time-resolved photoluminescence studies of CdTe solar cells. *J. Appl. Phys.* **2003**, *94*, 3549−3555.

(16) Ohnesorge, B.; Weigand, R.; Bacher, G.; Forchel, A.; Riedl, W.; Karg, F. Minority-carrier lifetime and efficiency of $Cu(In,Ga)Se_2$ solar cells. *Appl. Phys. Lett.* **1998**, *73*, 1224−1226.

(17) Gunawan, O.; Todorov, T. K.; Mitzi, D. B. Loss mechanisms in hydrazine-processed $Cu_2ZnSn(Se,S)_4$ solar cells. *Appl. Phys. Lett.* **2010**, *97*, 233506.

(18) Metzger, W. K.; Repins, I. L.; Romero, M.; Dippo, P.; Contreras, M.; Noufi, R.; Levi, D. Recombination kinetics and stability in polycrystalline $Cu(In,Ga)Se_2$ solar cells. *Thin Solid Films* **2009**, *517*, 2360−2364.

(19) Jackson, P.; Wuerz, R.; Hariskos, D.; Lotter, E.; Witte, W.; Powalla, M. Effects of heavy alkali elements in $Cu(In,Ga)Se_2$ solar cells with efficiencies up to 22.6%. *Phys. Status Solidi RRL* **2016**, *10*, 583−586.

(20) Chen, S.; Walsh, A.; Gong, X.-G.; Wei, S.-H. Classification of Lattice Defects in the Kesterite Cu_2ZnSnS_4 and $Cu_2ZnSnSe_4$ Earth-Abundant Solar Cell Absorbers. *Adv. Mater.* **2013**, *25*, 1522−1539.

(21) Chen, S.; Wang, L.-W.; Walsh, A.; Gong, X. G.; Wei, S.-H. Abundance of Cu_{Zn}+Sn_{Zn} and 2Cu_{Zn}+Sn_{Zn} defect clusters in kesterite solar cells. *Appl. Phys. Lett.* **2012**, *101*, 223901.

(22) Walsh, A.; Chen, S.; Wei, S.-H.; Gong, X.-G. Kesterite Thin-Film Solar Cells: Advances in Materials Modelling of Cu_2ZnSnS_4. *Adv. Energy Mater.* **2012**, *2*, 400−409.

(23) Han, D.; Sun, Y. Y.; Bang, J.; Zhang, Y. Y.; Sun, H.-B.; Li, X.-B.; Zhang, S. B. Deep electron traps and origin of *p*-type conductivity in the earth-abundant solar-cell material Cu_2ZnSnS_4. *Phys. Rev. B* **2013**, *87*, 155206.

(24) Biswas, K.; Lany, S.; Zunger, A. The electronic consequences of multivalent elements in inorganic solar absorbers: multivalency of Sn in Cu_2ZnSnS_4. *Appl. Phys. Lett.* **2010**, *96*, 201902.

(25) Grossberg, M.; Raadik, T.; Raudoja, J.; Krustok, J. Photoluminescence study of defect clusters in Cu_2ZnSnS_4 polycrystals. *Curr. Appl. Phys.* **2014**, *14*, 447−450.

(26) Shockley, W.; Read, W. T. Statistics of the Recombinations of Holes and Electrons. *Phys. Rev.* **1952**, *87*, 835.

(27) Hall, R. N. Electron-Hole Recombination in Germanium. *Phys. Rev.* **1952**, *87*, 387.

(28) Tsuchiya, T. Interactions between Interface Traps in Electron Capture/Emission Processes: Deviation from Charge Pumping Current Based on the Shockley−Read−Hall Theory. *Appl. Phys. Express* **2011**, *4*, 094104.

(29) Reshchikov, M. A.; Kvasov, A. A.; Bishop, M. F.; McMullen, T.; Usikov, A.; Soukhoveev, V.; Dmitriev, V. A. Tunable and abrupt thermal quenching of photoluminescence in high-resistivity Zn-doped GaN. *Phys. Rev. B* **2011**, *84*, 075212.

(30) Juršėnas, S.; Miasojedovas, S.; Kuriliik, G.; Žukauskas, A.; Hageman, P. R. Luminescence decay in highly excited GaN grown by hydride vapor-phase epitaxy. *Appl. Phys. Lett.* **2003**, *83*, 66−68.

(31) Huang, K.; Rhys, A. Theory of light absorption and non-radiative transitions in F-centres. *Proc. R. Soc. London, Ser. A* **1950**, *204*, 406−423.

(32) Freed, K. F.; Jortner, J. Multiphonon Processes in the Nonradiative Decay of Large Molecules. *J. Chem. Phys.* **1970**, *52*, 6272−6291.

(33) Kubo, R.; Toyozawa, Y. Application of the Method of Generating Function to Radiative and Non-Radiative Transitions of a Trapped Electron in a Crystal. *Prog. Theor. Phys.* **1955**, *13*, 160−182.

(34) Lax, M. The Franck-Condon Principle and Its Application to Crystals. *J. Chem. Phys.* **1952**, *20*, 1752−1760.

DOI: 10.1021/acs.chemmater.8b03933
Chem. Mater. 2019, 31, 826−833

(35) Rickayzen, G.; Fröhlich, H. On the theory of the thermal capture of electrons in semi-conductors. *Proc. R. Soc. London, Ser. A* **1957**, *241*, 480−494.
(36) Bonch-Bruevich, V. L.; Landsberg, E. G. Recombination Mechanisms. *Phys. Status Solidi B* **1968**, *29*, 9−43.
(37) Stoneham, A. M. *Theory of Defects in Solids: Electronic Structure of Defects in Insulators and Semiconductors*; Oxford University Press: Oxford, U.K., 2001, DOI: 10.1093/acprof:oso/9780198507802.001.0001.
(38) Gummel, H.; Lax, M. Thermal capture of electrons in silicon. *Ann. Phys.* **1957**, *2*, 28−56.
(39) Shi, L.; Wang, L.-W. *Ab initio* Calculations of Deep-Level Carrier Nonradiative Recombination Rates in Bulk Semiconductors. *Phys. Rev. Lett.* **2012**, *109*, 245501.
(40) Shi, L.; Xu, K.; Wang, L.-W. Comparative study of *ab initio* nonradiative recombination rate calculations under different formalisms. *Phys. Rev. B* **2015**, *91*, 205315.
(41) Zhang, H.-S.; Shi, L.; Yang, X.-B.; Zhao, Y.-J.; Xu, K.; Wang, L.-W. First-Principles Calculations of Quantum Efficiency for Point Defects in Semiconductors: The Example of Yellow Luminance by GaN: C_N+O_N and GaN:C_N. *Adv. Opt. Mater.* **2017**, *5*, 1700404.
(42) Alkauskas, A.; Yan, Q.; Van de Walle, C. G. First-principles theory of nonradiative carrier capture via multiphonon emission. *Phys. Rev. B* **2014**, *90*, 075202.
(43) Alkauskas, A.; Dreyer, C. E.; Lyons, J. L.; Van de Walle, C. G. Role of excited states in Shockley-Read-Hall recombination in wide-band-gap semiconductors. *Phys. Rev. B* **2016**, *93*, 201304.
(44) Barmparis, G. D.; Puzyrev, Y. S.; Zhang, X.-G.; Pantelides, S. T. Theory of inelastic multiphonon scattering and carrier capture by defects in semiconductors: Application to capture cross sections. *Phys. Rev. B* **2015**, *92*, 214111.
(45) Yang, J.-H.; Shi, L.; Wang, L.-W.; Wei, S.-H. Non-Radiative Carrier Recombination Enhanced by Two-Level Process: A First-Principles Study. *Sci. Rep.* **2016**, *6*, 21712.
(46) Yang, J.-H.; Metzger, W. K.; Wei, S.-H. Carrier providers or killers: The case of Cu defects in CdTe. *Appl. Phys. Lett.* **2017**, *111*, 042106.
(47) Li, J.; Zhu, H.-F.; Zhang, Y.-Y.; Yuan, Z.-K.; Chen, S.; Gong, X.-G. Large carrier-capture rate of Pb_I antisite in $CH_3NH_3PbI_3$ induced by heavy atoms and soft phonon modes. *Phys. Rev. B* **2017**, *96*, 104103.
(48) Henry, C. H.; Lang, D. V. Nonradiative capture and recombination by multiphonon emission in GaAs and GaP. *Phys. Rev. B* **1977**, *15*, 989.
(49) Todorov, T. K.; Reuter, K. B.; Mitzi, D. B. High-Efficiency Solar Cell with Earth-Abundant Liquid-Processed Absorber. *Adv. Mater.* **2010**, *22*, E156−E159.
(50) Barkhouse, D. A. R.; Gunawan, O.; Gokmen, T.; Todorov, T. K.; Mitzi, D. B. Device characteristics of a 10.1% hydrazine-processed $Cu_2ZnSn(Se,S)_4$ solar cell. *Prog. Photovoltaics* **2012**, *20*, 6−11.
(51) Shin, B.; Gunawan, O.; Zhu, Y.; Bojarczuk, N. A.; Chey, S. J.; Guha, S. Thin film solar cell with 8.4% power conversion efficiency using an earth-abundant Cu_2ZnSnS_4 absorber. *Prog. Photovoltaics* **2013**, *21*, 72−76.
(52) Todorov, T.; Gunawan, O.; Chey, S. J.; de Monsabert, T. G.; Prabhakar, A.; Mitzi, D. B. Progress towards marketable earth-abundant chalcogenide solar cells. *Thin Solid Films* **2011**, *519*, 7378−7381.
(53) Pässler, R. Relationships between the nonradiative multiphonon carrier-capture properties of deep charged and neutral centres in semiconductors. *Phys. Status Solidi B* **1976**, *78*, 625−635.
(54) Huang, K. Lattice relaxation and theory of multiphonon transitions. *Prog. Phys.* **1981**, *1*, 31.
(55) Heyd, J.; Scuseria, G. E.; Ernzerhof, M. Hybrid functionals based on a screened Coulomb potential. *J. Chem. Phys.* **2003**, *118*, 8207−8215.
(56) Heyd, J.; Scuseria, G. E.; Ernzerhof, M. Erratum:"Hybrid functionals based on a screened Coulomb potential"[J. Chem. Phys. 118, 8207 (2003)]. *J. Chem. Phys.* **2006**, *124*, 219906.
(57) Perdew, J. P.; Burke, K.; Ernzerhof, M. Generalized Gradient Approximation Made Simple. *Phys. Rev. Lett.* **1996**, *77*, 3865.
(58) Kresse, G.; Furthmüller, J. Efficient iterative schemes for *ab initio* total-energy calculations using a plane-wave basis set. *Phys. Rev. B* **1996**, *54*, 11169.
(59) Blöchl, P. E. Projector augmented-wave method. *Phys. Rev. B* **1994**, *50*, 17953.
(60) Giannozzi, P.; Baroni, S.; Bonini, N.; Calandra, M.; Car, R.; Cavazzoni, C.; Ceresoli, D.; Chiarotti, G. L.; Cococcioni, M.; Dabo, I.; Dal Corso, A.; de Gironcoli, S.; Fabris, S.; Fratesi, G.; Gebauer, R.; Gerstmann, U.; Gougoussis, C.; Kokalj, A.; Lazzeri, M.; Martin-Samos, L.; Marzari, N.; Mauri, F.; Mazzarello, R.; Paolini, S.; Pasquarello, A.; Paulatto, L.; Sbraccia, C.; Scandolo, S.; Sclauzero, G.; Seitsonen, A. P.; Smogunov, A.; Umari, P.; Wentzcovitch, R. M. QUANTUM ESPRESSO: a modular and open-source software project for quantum simulations of materials. *J. Phys.: Condens. Matter* **2009**, *21*, 395502.
(61) Wei, S.-H. Overcoming the doping bottleneck in semiconductors. *Comput. Mater. Sci.* **2004**, *30*, 337−348.
(62) Zhang, S. B.; Wei, S.-H.; Zunger, A.; Katayama-Yoshida, H. Defect physics of the $CuInSe_2$ chalcopyrite semiconductor. *Phys. Rev. B* **1998**, *57*, 9642.
(63) Lany, S.; Zunger, A. Assessment of correction methods for the band-gap problem and for finite-size effects in supercell defect calculations: Case studies for ZnO and GaAs. *Phys. Rev. B* **2008**, *78*, 235104.

DOI: 10.1021/acs.chemmater.8b03933
Chem. Mater. 2019, 31, 826−833